



# Energy, exergy and economic analysis of utilizing the supercritical CO<sub>2</sub> recompression Brayton cycle integrated with solar energy in natural gas city gate station

Amir Hossein Shokouhi Tabrizi<sup>1</sup> · Hamid Niazmand<sup>1</sup> · Mahmood Farzaneh-Gord<sup>1</sup> · Amir Ebrahimi-Moghadam<sup>2</sup>

Received: 10 June 2020 / Accepted: 12 September 2020 / Published online: 9 October 2020  
© Akadémiai Kiadó, Budapest, Hungary 2020

## Abstract

The pressure of natural gas stream must be reduced in city gas station. The natural gas has to be preheated before pressure reduction takes place usually through throttling valves. In conventional city gas stations, the natural gas is preheated by indirect water bath heaters, which burn a large amount of the natural gas as fuel. In this study, the rejected heat from a supercritical carbon dioxide recompression cycle using solar energy is recovered for preheating the natural gas. The novel design of this system generates uniform electricity as well as preheats the natural gas in city gate station. The proposed system is simulated for Birjand city gas station as a case study, and a thorough techno-economic analysis is performed in Engineering Equation Solver for evaluating the system performance. The results of this study demonstrate that parabolic trough collectors with 25 rows are the most efficient solar system while the annual average of thermal and exergy efficiency of the system is 0.56 and 0.41, respectively. The exergetic analysis of the system shows that the highest average exergy destruction takes place in the throttling valve and the second highest in the solar collectors. Also, the total amount of fuel saving is estimated at 4.87 million cubic meters annually and the net power output is equal to 2.86 MW. From the economic point of view, the value of the payback period is estimated 4 years and, based on the net present value method, after 8 years, the initial investment could be returned.

**Keywords** s-CO<sub>2</sub> recompression cycle · Solar energy · LS-3 collectors · Natural gas city gate station · Brayton cycle · Techno-economic analysis · Parabolic trough collector

## List of symbols

$A$	Area, m <sup>2</sup>	$F'$	Collector efficiency factor
$B_d$	Daily direct solar radiation, J m <sup>-2</sup> day <sup>-1</sup>	$F''$	Collector flow factor
$C_p$	Specific heat capacity, J kg <sup>-1</sup> K <sup>-1</sup>	$G_b$	Beam solar radiation, W m <sup>-2</sup>
CI	Cost index	$G_{sc}$	Solar constant, W m <sup>-2</sup>
CGS	City gas station	$h$	Specific enthalpy, kJ kg <sup>-1</sup>
$D$	Diameter, m	$h_{i,c}$	Heat transfer coefficient inside the coil, W m <sup>-2</sup> K <sup>-1</sup>
$D_d$	Daily diffuse solar radiation, J m <sup>-2</sup> day <sup>-1</sup>	$h_{o,c}$	Heat transfer coefficient outside the coil, W m <sup>-2</sup> K <sup>-1</sup>
DNI	Direct normal irradiance	$h_{i,t}$	Heat transfer coefficient inside the tube, W m <sup>-2</sup> K <sup>-1</sup>
$\dot{E}$	Exergy rate	$H$	Daily total solar radiation, J m <sup>-2</sup> day <sup>-1</sup>
$f$	Focal length, m	$H_o$	Daily extraterrestrial solar radiation, J m <sup>-2</sup> day <sup>-1</sup>
$F_R$	Heat removal factor	$i$	Discount rate, %
		$k$	Thermal conductivity, W m <sup>-1</sup> K <sup>-1</sup>
		$K_T$	Clearness index
		$K(\theta)$	Incident angle modifier
		$L$	Length, m
		$L_s$	Distance between two parallel collectors, m

✉ Mahmood Farzaneh-Gord  
m.farzanehgord@um.ac.ir

<sup>1</sup> Faculty of Engineering, Mechanical Engineering Department, Ferdowsi University of Mashhad, Mashhad, Iran

<sup>2</sup> Faculty of Mechanical Engineering, Shahrood University of Technology, Shahrood, Iran

LHV	Lower heating value, $\text{J kg}^{-1}$
$\dot{m}$	Mass flow rate, $\text{kg s}^{-1}$
NG	Natural gas
$n$	Number of date
$P$	Pressure, kPa
PTC	Parabolic trough collector
$R_f$	Fouling thermal resistance, $\text{m}^2 \text{K W}^{-1}$
$R_t$	Net cash inflow–outflow, \$
$S$	Heat absorbed, $\text{W m}^{-2}$
SR	Solar receiver
SCRBC	Supercritical carbon dioxide recompression Brayton cycle
$Q_u$	Useful energy, W
$t$	Number of time period
$T$	Temperature, $^{\circ}\text{C}$
$U$	Overall heat transfer coefficient, $\text{W m}^{-2} \text{K}^{-1}$
$W$	Width, m

### Greek symbols

$\alpha_r$	Receiver absorptivity
$\gamma$	Intercept factor
$\Delta$	Difference
$\delta$	Declination angle, $^{\circ}$
$\varepsilon$	Effectiveness
$\eta$	Efficiency
$\theta$	Incidence angle, $^{\circ}$
$\theta_z$	Zenith angle, $^{\circ}$
$\mu$	Viscosity, Pa s
$\rho$	Density, $\text{kg m}^{-3}$
$\rho_m$	Collector reflectance
$\tau$	Transmissivity
$\tau_b$	Atmospheric transmittance
$\phi$	Latitude location, $^{\circ}$
$\psi$	Exergy flow
$\omega$	Hour angle, $^{\circ}$
$\omega_s$	Sunset hour angle, $^{\circ}$

### Subscripts

0	Environment state
1,2,3,...	Cycle states
a	Aperture
abs	Absorber
amb	Ambient
c	Coil
comp	Compressor
ex	Exergy
f	Fuel
h	Heater
HE	Heat exchanger
hyd	Hydrate
i	Inlet, inside
o	Outlet, outside
opt	Optical
new	New

NG	Natural gas
$\text{NG}_1$	Natural gas before heater
$\text{NG}_2$	Natural gas after heater
$\text{NG}_3$	Natural gas after throttling valve
L	Loss
pum	Pump
rec	Recuperator
ref	Reference
s	Solar
th	Thermal
TV	Throttling valve
tur	Turbine
w	Water

## Introduction

Natural gas (NG) as the largest fossil fuel source is transferred with a high pressure (about 5–7 MPa) to overcome pressure loss related to the long way that gas should pass from a refinery to consumption points such as power plants and city entrances [1]. Due to the lower required pressure for using the NG in domestic and industrial applications, the NG pressure should be decreased at consumption points. City gate stations (CGSs) are installed at the consumption zone entrances to reduce pressure. At CGSs, the pressure is usually reduced to 1.5–2 MPa [2]. Currently, throttle valves carry out this mission where the constant-enthalpy expansion happens, and a significant amount of energy is lost [3]. It has a negative impact on the environment by increasing concentration of carbon dioxide in the atmosphere. As a result, some solution has been studied to absorb carbon dioxide and store it [4]. Also, a valuable pressure exergy destroyed at exit of the pressure reduction process [5]. As the NG Joule–Thomson coefficient is positive, reducing its pressure causes to a temperature drop. The NG temperature should not be lower than a minimum value. This minimum value for temperature is called hydrate forming temperature, which depends on the NG pressure and compositions [3]. The hydrate formation zone is a region where the water droplets, which are suspended in the NG, start freezing and cause the corrosion and clogging of pipes [6]. To prevent this scenario, the NG stream needs to be warmed up to a particular level before the pressure reduction process. Indirect water bath heaters are used in the CGS to preheat the NG in advance. This type of heaters has a main problem, which they need a huge amount of gas to provide the required heat for heating the gas stream before the process of pressure reduction [7]. That is the reason that the performance of a CGS is not satisfactory. There is complete literature about the research projects around gas pressure reduction points, mainly discussed on the two topics of the minimization of the energy and consumption of the water bath heater and

energy recovery. In this field of study, firstly, Farzaneh-Gord et al. [8] proposed solar energy (as a renewable energy resource) for supplying a part of the required heating energy in CGSs. Farzaneh-Gord et al. [9] made remarkable effort to use solar systems in Sari (a city in northern Iran). They designed a solar system which utilized solar collectors and hot water storage tanks to store a part of the required heat during the day for using during the night. The system included a storage tank with a capacity of 45 m<sup>3</sup> and an array of 450 solar collectors. It was shown that fuel consumption could be reduced about 14%, whereas the first design [8] could save 11%. In another study, Farzaneh-Gord et al. [10] used an automatically controlled heater in CGSs instead of the conventional linear heater and compared this system's thermal behavior to other proposed systems and discovered the latter is superior. The same research team [11] employed geothermal energy instead of burning fuels in heaters for preheating the NG. They applied some economical methods such as net present value (NPV) and internal rate of return (IRR) in their analysis.

In some other investigations in this field, turbo-expanders and cogeneration systems have been proposed to enhance the performance of the CGSs. Energetic and exergetic analysis on the systems which are suggested in these studies showed that there is a considerable improvement potential in the first law and the second-law efficiencies of the CGSs. Farzaneh-Gord et al. [12] conducted a detailed study on a combined heat and power system. The results show that the amount of power generation in seven Khorasan province (in Iran) CGS by cogeneration is equal to 20.5 MW annually. Borelli et al. [13] used a pair of turbo-expanders to reduce the NG pressure in two stages. They simulated the dynamic performance of the pressure reduction station (PRS) numerically and showed that the two-stage process uses lower energy to preheat the NG compared to the conventional single-stage pressure reduction process. Xiong et al. [14] showed that some portion of NG energy can be harvested during the pressure reduction, if the throttling valve is removed and a single screw expander is used instead of it in a PRS. They also found that if the daily power output and daily exergy efficiency reach about 61 kWh and 37%, the daily round-trip efficiency of the system will enhance more than 25%. Olfati et al. [15] modeled the NG reduction process in a CGS and made an analysis which was based on different seasonal strategies in order to explore the exergetic and energetic losses of the heater by considering the heater stack as the main source of loss. In another study, Olfati et al. [16] modeled operation of the CGS regulator and calculated minimum temperature of NG for preheating according to regulator outlet temperature. Their results showed that the modified station has energy consumption and exergy destruction at least 33% and 15%, respectively. Ashouri et al. [17] studied how the tube arrangement can affect the water bath heaters

thermal performance, and it was deduced that the vertical and horizontal pitches have significant effects, and the thermal performance of the heater can be enhanced by optimum design. Salari and Goudarzi [18] investigated the effect of coiled wire tube insert as a turbulator in order to increase heat transfer in Mokhtar city gate station heater. They simulated the turbulator in two states of circular and elliptical tubes through ANSYS CFX so as to examine the performance of geometrical parameter of it. The results indicated that the best performance belongs to the tube with elliptical cross section with diameters ration of 0.95 and the spring tube insert with diameter ratio of 10. In another study, Salari and Goudarzi [19] used computational fluid dynamics (CFD) approach and employed different kinds of coiled wires in order to intensify the heat transfer in a water bath heater. Their results showed that and improvement of 62%, 79% and 57% in the thermal efficiency is occurred for the heaters with square, triangular and circular cross sections, respectively. Rahmati and Reiszadeh [6] experimentally investigated the effects of using multi-walled carbon nanotubes on improving the heat transfer rate in CGS. They concluded that up to 48% increment in the thermal efficiency of the heater is occurred by applying their proposed system. In a recently published work, Khosravi et al. [20] proposed a new design of CGS's heat pipes (twisted flow disturber) for increasing the heat transfer coefficient and subsequently increasing the thermal efficiency of the heater. The results show that using the flow disturber may improve the average Nusselt number of the gas flow through the coil by about 20%, reducing fuel consumption of the heater and increasing its thermal efficiency.

The growing energy demand, the increased consumption of the fossil fuel and the population growth have become one of the most important issues over the past years. Renewable energy sources such as solar energy can be good alternatives to conventional fuel sources [21]. The integration of parabolic solar collectors with supercritical carbon dioxide recompression Brayton cycle has a good potential for power generation of the future, and it has attracted a lot of attention nowadays. Qiu et al. [22] established an integrated numerical model to solve the complex energy transfer in a parabolic trough collector using supercritical carbon dioxide as heat transfer fluid by combining Monte Carlo ray tracing and finite volume method. The results show that the solar fluxes on the receiver walls were non-uniform, the optical efficiency at normal incidence was 84.19% and the temperature difference of the absorber was obtained in the range of 18–60 K under typical conditions. Bellos and Tzivanidis [23] investigated the utilization of supercritical carbon dioxide in parabolic trough collector for various operating conditions. They performed a parametric analysis of the collector by examining the inlet temperature, pressure and mass flow rate with a model in EES. The results indicate that the maximum exergetic efficiency of the collector is equal to

45.3% for inlet temperature 750 K. In another study, Wang et al. [24] developed a new simulation model of a recompression supercritical carbon dioxide Brayton cycle, using parabolic trough solar collectors. They examined the effects of the compressor outlet pressure, turbine inlet temperature and cooling temperature on the performance of the proposed cycle and concluded that increasing the turbine inlet pressure reduces the efficiency, where increasing the turbine inlet temperature increases the efficiency, and there is a critical cooling temperature point in which the cycle efficiency reaches a maximum value of 0.4, but drops after this point.

In this study, for the first time, the utilization of supercritical carbon dioxide recompression Brayton cycle (SCRBC) integrated with solar energy as a high-temperature heat source in the natural gas pressure drop station is proposed and analyzed. The analysis is performed with engineering equation solver (EES). For a first time in this field, the rejected heat from the Brayton cycle is proposed to preheat the natural gas steam, while the electricity is generated in the CGS at the same time. Utilizing solar energy as a renewable energy source reduces the environmental pollution by decreasing the amount of fuel consumption. Also, burning natural gas in the Brayton cycle (using an auxiliary boiler to keep turbine inlet temperature constant) rather than current CGS heaters with low thermal efficiency improves performance of the natural gas pressure drop station. The Birjand CGS in Iran is selected as a case study to evaluate the efficiency and performance of the proposed system. A comprehensive energy, exergy and economic analysis of suggested configuration is investigated. The two most essential criteria of payback period and net present value are utilized for economic evaluation.

## Natural gas pressure reduction station (CGS)

### The current CGS

The high pressure of the NG has to be decreased to a lower pressure level when an NG pipeline approaches a city. This aim could be achieved using an NG CGS. In order to reduce the gas pressure, throttling valves are used. A detailed schematic diagram of the current CGS is illustrated in Fig. 1. The temperature and pressure of the inlet NG into the CGS are related to the surrounding temperature. A severe temperature drop has occurred during the pressure reduction process, and hence, the NG should be preheated before the gas passes throughout the throttle valves. The NG preheating is done to ensure that it stays above the dew point and hydrate formation zone so as not to solid or liquid phase condenses at the output temperature. The standard range of the preheated gas temperature is in the range of 30–55 °C, but the value of it depends on the inlet pressure and temperature. The indirect water bath heaters, which are known as line heaters, are used as heat exchangers in NG pressure reduction station and are shown in Fig. 1. The heaters are contained of four basic components, including the fire tube, the heater shell, the water expansion section and the gas coil. The heater shell is surrounding the gas coil, the water bath and the fire tube. The duty of a fire tube, which burns NG, is to provide heat to water, which plays an intermarriage fluid role. After that, the water has to transfer heat to NG, which is flowing throughout a coil that is immersed in the water. When the water bath is heated, the expanded water flows into the expansion tank that is located above of the heater [10].

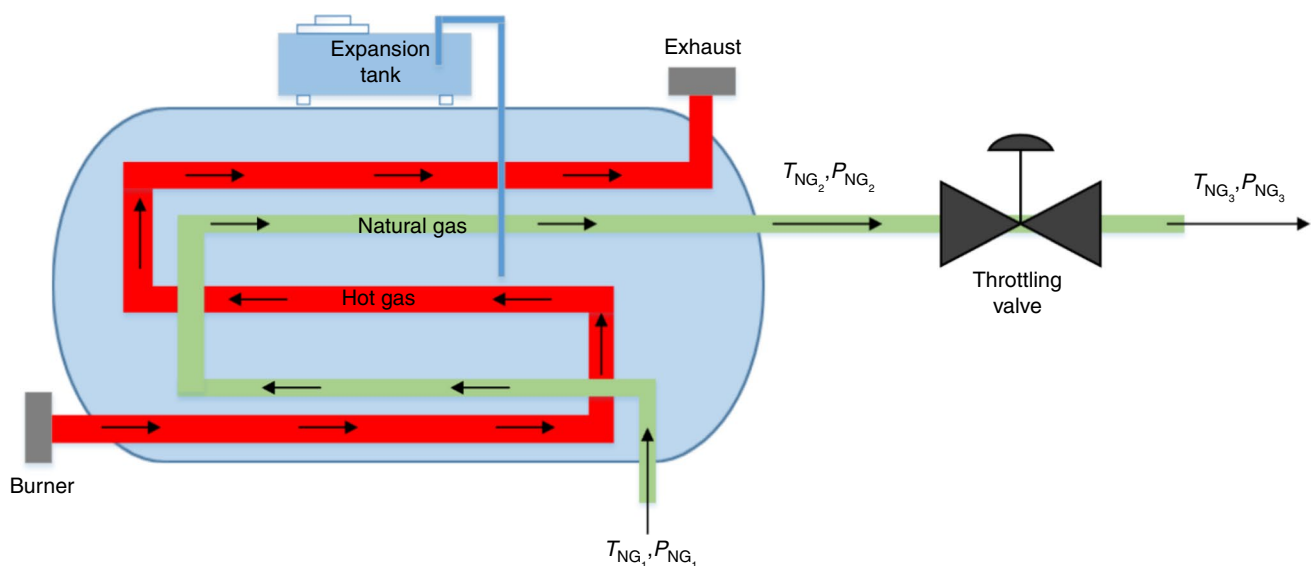


**Fig. 1** Schematic diagram of indirect water bath heater employed in CGS for preheating natural gas

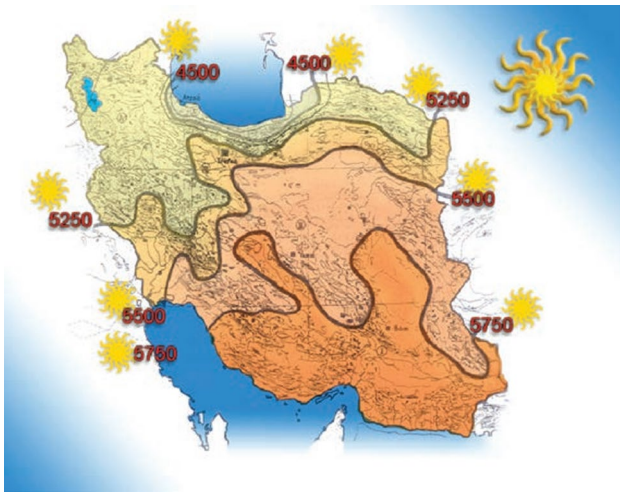


Fig. 2 Daily average of solar radiation zones for Iran ( $\text{Wh m}^{-2}$ ) [26]

### The case study

Iran is situated in Western Central Asia and is placed between 25 and 38° N latitudes and 44 and 62° E longitudes. The central and southern zones of Iran are considered as one of the warmest zones of the world. As observed in Fig. 2, Iran has a high potential for utilizing solar energy as heating systems. The local climate of Iran and geographical location are important reasons for using this energy. The Birjand station with a maximum capacity of  $60,000 \text{ Sm}^3 \text{ h}^{-1}$  is considered as the case study. Birjand is the capital of the Iranian Province of South Khorasan, which has the latitude and longitude angles of 32° N and 59° E. It is situated near an area which is named Dashte-Lut desert. It is one of the best places in the world in terms of the total received solar irradiation per year, and hence, it has a high potential to install solar heating systems compared to the other cities of Iran [25]. Birjand's CGS contains two separate heaters in order to provide the needed heat to warm up the NG flows with the volume flow rate of  $30,000 \text{ Sm}^3 \text{ h}^{-1}$ . Table 1 reports more details about Birjand CGS heaters, and Table 2 shows the component mole fraction and mass fraction of the natural gas stream. The case study is selected mainly due to financial support from the regional NG company.

### The proposed system

The integration of supercritical carbon dioxide recompression Brayton cycle (SCRBC) with parabolic solar collectors has a good potential for power generation of the future, and it has attracted a lot of attention nowadays. So far, recovering the rejected heat from the solar SCRBC has not been utilized for CGSs in the previous studies. When a CGS needs heat with low temperature, exited heat from the recompression

Table 1 Equipment specification of Birjand CGS heater

Characteristics	Value
Maximum natural gas flow rate/ $\text{Sm}^3 \text{ h}^{-1}$	60,000
Natural gas inlet pressure/MPa	5.9
Natural gas outlet pressure/MPa	1.8
Water capacity/ $\text{m}^3$	36
Surface area of fire tube/ $\text{m}^2$	88.1
Diameter of coils/m	0.1
Wall thickness of coils/mm	8.56
Number of coils	2
Shell diameter/m	2.85
Shell length/m	10
Maximum bath temperature/ $^{\circ}\text{C}$	88
Maximum heating duty/kW	1750

Brayton cycle can be used for preheating the NG to save a significant amount of fuel. Carbon dioxide is used as the working fluid in the SCRBC, which is a closed-loop Brayton cycle, and it is operated between low pressure near the critical point of CO<sub>2</sub> (7.4 MPa and 31 °C) and high pressure about 20 MPa [27]. The SCRBC is a kind of a power conversion system that can combine the advantages of a gas turbine system and a steam Rankine cycle [28]. It has been suggested as a power cycle for parabolic trough solar receivers owing to the following advantages [29–31]:

- Carbon dioxide is non-toxic and non-flammable.
- Carbon dioxide is easily found in nature, with low cost and without severe environmental effects in low quantities.
- Carbon dioxide is a single phase during the heating and cooling process.
- The cycle has low compression work and a high thermal efficiency.
- Wasting heat rejection occurs in higher temperatures.
- Capital cost of the Brayton cycle is less than other thermodynamic cycles.

A schematic of the proposed system and T-s diagram are shown in Figs. 3 and 4. The system is composed of a CGS, a solar field and a supercritical carbon dioxide recompression Brayton cycle.

The SCRBC improves thermal efficiency by reducing the heat rejection from the cycle through the using a second compressor (recompression compressor) before the heat exchanger. Carbon dioxide is split into two parts. The large part of the carbon dioxide (is shown with  $x$  in Fig. 3) fed into the main compressor (state 1) at critical conditions due to high density and heat capacity near its critical point [32] and compresses to high pressure (20 MPa). Subsequently, the flow preheated through low-temperature recuperator

**Table 2** Birjand natural gas compositions

Components	CH <sub>4</sub>	C <sub>2</sub> H <sub>6</sub>	C <sub>3</sub> H <sub>8</sub>	i-C <sub>4</sub> H <sub>10</sub>	n-C <sub>4</sub> H <sub>10</sub>	i-C <sub>5</sub> H <sub>12</sub>	n-C <sub>5</sub> H <sub>12</sub>	CO <sub>2</sub>	N <sub>2</sub>
Mole fraction/%	98.221	0.415	0.053	0.011	0.026	0.012	0.002	0.677	0.583
Mass fraction/%	95.914	0.760	0.142	0.039	0.092	0.053	0.009	1.814	1.177

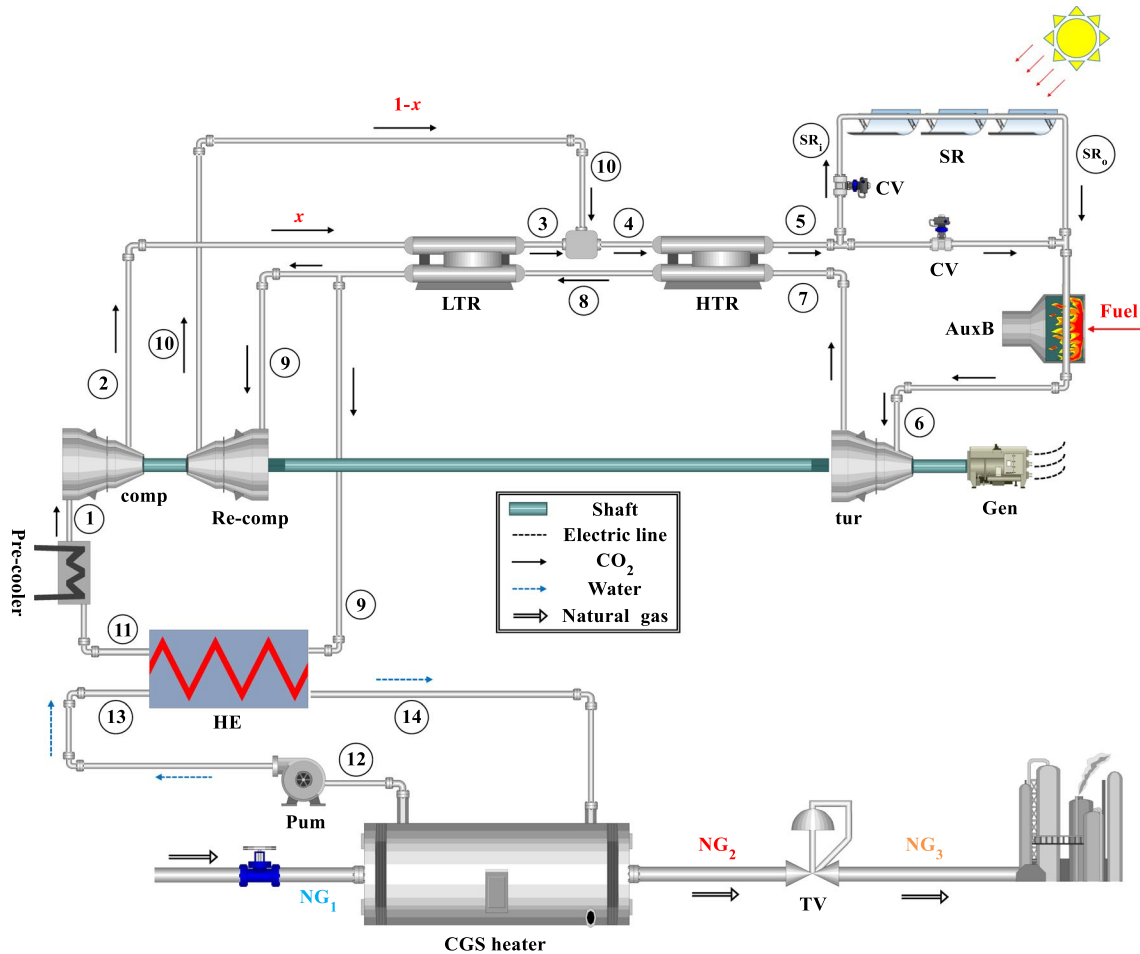


**Fig. 3** Schematic diagram of the proposed system

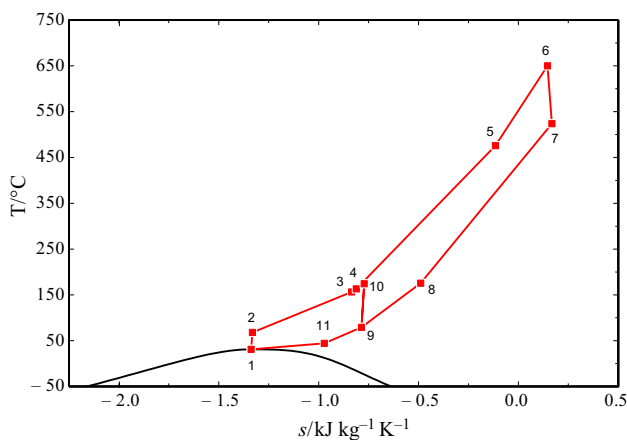


**Fig. 4** T-s diagram of the proposed system

(state 3) to blend with the outlet of the recompression compressor (state 10). The entire carbon dioxide (state 4) is preheated furthermore in the high-temperature recuperator (state 5) and send to the solar filed. The solar energy can be employed for many usages. This energy is one of the best alternatives for fossil fuels [10]. There are three main types of collectors that are able to absorb heat. In the current study, parabolic trough collector (PTC) type of LS-3 is considered for installation which has been commercially proved. The advantages of PTCs are their lower thermal losses, higher efficiency at higher temperature, the smaller collecting surface in comparison with other collectors for a certain power requirement and the most mature concentrated solar power technology. Some disadvantage of the PTCs is its higher solar tracking and maintenance costs,

interrupting their operation at very high wind speeds. PTCs can only utilize direct solar radiation, which is called direct normal irradiance (DNI) or beam radiation. In other words, DNI is the solar radiation fraction that is not deviated by clouds, dust or fumes in the atmosphere and also that reaches the surface of Earth as a parallel beam [33]. The duty of PTCs is to focus direct solar radiation onto a central line on the collector axis. A receiver tube is installed in this focal line, which has a fluid flowing inside that. It absorbs the focused solar energy from the tube wall. The collector is considered east–west single-axis tracking in order that the solar beam falls parallel to its axis. PTCs are taken into account as the demanding temperature for this study (up to 650 °C). In this temperature range, solar dish collectors can be employed. Lack of flexibility, high cost, required a large area of land and number of equipment are some reasons not to utilize this type of collector for the present study [34]. By keeping the inlet temperature of the turbine constant in proposed system (state 6), an auxiliary boiler is required to raise the temperature of carbon dioxide during the day as well as night when solar energy is unavailable. After that, high-temperature CO<sub>2</sub> flows into the turbine, and while producing power, its pressure expands to the inlet pressure of the both compressors (state 7). The fluid exiting the turbine is cooled in the high and low-temperature recuperator (states 8–9), in which the available heat is transferred to the high pressure side. After leaving the low-temperature recuperator flow is split. The large fraction of the flow enters the heat exchanger to preheat NG and is cooled in the precooler to the inlet temperature of main compressor (state 11), and the other recompresses to the high pressure (state 10).

## Modeling

### Energy demand in natural gas pressure reduction station

The heating duty of the heater and the water bath temperature could be calculated with determining the temperatures and pressures of the inlet and outlet NG streams. The temperature of gas hydrate ( $T_{\text{hyd}}$ ) could be computed from thermodynamics models by knowing the compositions of NG and standard outlet station gas pressure (250 psi or 1.7 MPa). Then, the temperature of the outlet gas stream is chosen to be 5 °C higher than the hydrate temperature [35]. Once the temperature of the outlet station gas stream is known, the heater exit gas temperature could be expressed as follows:

$$T_{\text{NG}_2} = T_{\text{hyd}} + 5 + \Delta T_{\text{TV}} \quad (1)$$

where  $\Delta T_{\text{TV}}$  is the temperature drop due to the pressure drop through the throttling valves. The value of temperature drop is determined by the pressure of the gas at the station inlet and the NG compositions. By knowing the heater exit gas temperature (and pressure), the heating duty of heater could be calculated as:

$$\dot{Q}_{\text{Heater}} = \dot{m}_{\text{NG}} (h_{\text{NG}_2} - h_{\text{NG}_1}) \quad (2)$$

It should be noted that the inlet pressure of CGS (heater) is measured and considered to be known. The gas temperature is considered as equal as the soil temperature because the gas passes a long distance through a buried pipeline at a depth of 1.5 m before it reaches the station [36]. The soil temperature depends on the ambient temperature and locations area. Najafimoud et al. [37] suggested an experimental formula that connects ambient temperature to the soil temperature at various depths. The soil temperature (°C) for depth more than 1 m height for Iran could be estimated as follows [37]:

$$T_{\text{NG}_1} = T_{\text{Soil}} = 0.0084 T_{\text{amb}}^2 + 0.3182 T_{\text{amb}} + 11.403 \quad (3)$$

The NG is utilized as a fuel in order to supply the heating duty of the water bath heater. By knowing thermal efficiency ( $\eta_{\text{h}}$ ) of the heater, the mass flow rate of fuel  $\dot{m}_{\text{f}}$  could be obtained as:

$$\dot{m}_{\text{f}} = \frac{\dot{Q}_{\text{Heater}}}{\eta_{\text{h}} \text{LHV}} \quad (4)$$

where LHV is the lower heating value of the NG as fuel. It is worth mentioning that the amount of the rejected heat from the heater to the surrounding is applied by defining a heater thermal efficiency. The current heaters operate with low thermal efficiencies between 0.35 and 0.5 [36]. In this study, heater thermal efficiency is considered to be 0.4. The gas coil in the heater is covered by water, and it could be simulated as internal flow in the constant temperature external fluid (here water) [36]. For this case, Incropera [38] express the equation below:

$$\frac{T_{\text{w}} - T_{\text{NG}_2}}{T_{\text{w}} - T_{\text{NG}_1}} = \exp\left(\frac{-\pi D_{\text{o,c}} L_{\text{c}} U_{\text{c}}}{\dot{m}_{\text{NG}} c_{\text{p,NG}}}\right) \quad (5)$$

where  $D_{\text{o}}$  is external diameter,  $L_{\text{c}}$  is the length of the coil and  $U_{\text{c}}$  is overall coil heat transfer coefficient. Solving the above equation for  $T_{\text{w}}$ , the above relation can be rewritten as follows:

$$T_{\text{w}} = \frac{T_{\text{NG}_2} - T_{\text{NG}_1} \exp\left(\frac{-\pi D_{\text{o,c}} L_{\text{c}} U_{\text{c}}}{\dot{m}_{\text{NG}} c_{\text{p,NG}}}\right)}{1 - \exp\left(\frac{-\pi D_{\text{o,c}} L_{\text{c}} U_{\text{c}}}{\dot{m}_{\text{NG}} c_{\text{p,NG}}}\right)} \quad (6)$$

The following equation is obtained to estimate the overall coil heat transfer coefficient:

$$\frac{1}{U_c} = \frac{D_o}{D_i h_i} + R_f + \frac{\frac{D_o}{2} \text{Ln} \frac{D_o}{D_i}}{k_c} + R_f + \frac{1}{h_o} \tag{7}$$

where  $h_i$  and  $h_o$  are the internal and external heat transfer coefficients of the coil,  $R_f$  is coil fouling thermal resistances of the coil,  $D_i$  and  $D_o$  are internal and external coil diameters and  $k_c$  is thermal conductivity of the coil. According to the properties of used water bath heaters, the overall coil heat transfer coefficient is equal to  $568 \text{ W m}^{-2} \text{ K}^{-1}$ .

### Solar radiation and parabolic trough collector

This section discusses energy analysis of the PTC. Carbon dioxide as heat transfer fluid circulates in the solar field, absorbs solar radiation and flows into SCRBS. The pressure drops in solar collectors are neglected. The heat losses from the PTCs solar field are divided into two parts, including losses from collectors and pipes. The useful energy is defined as differences between absorbed energy by a solar collector and heat losses which is transferred to the working fluid, and it can be calculated by the equation below [39]:

$$Q_u = F_R A_a \left[ S - \frac{A_r}{A_a} U_L (T_i - T_a) \right] - Q_{L, \text{pipe}} \tag{8}$$

where  $A_a$  is the aperture area,  $A_r$  is the receiver area,  $F_R$  is the heat removal factor,  $S$  is the heat absorbed by the receiver,  $U_L$  is the solar collector overall heat loss coefficient,  $T_i$  is the receiver inlet temperature,  $T_a$  is the ambient temperature and  $Q_{L, \text{pipe}}$  is the thermal losses from pipes. The heat absorbed by the receiver is given by [40]:

$$S = G_b K(\theta) \eta_{\text{opt}} \eta_{\text{row-shading}} \eta_{\text{end-loss}} F_e \cos \theta \tag{9}$$

where  $G_b$  is the beam solar radiation,  $\theta$  is the angle of incident (deg),  $K(\theta)$  is the incident angle modifier,  $\eta_{\text{opt}}$  is the optical efficiency,  $\eta_{\text{row shading}}$  is the row shading factor,  $\eta_{\text{end loss}}$  is the end losses factor and  $F_e$  is the mirror cleanliness.

The beam solar radiation can be evaluated by the following expression [41]:

$$G_b = G_{sc} \left( 1 + 0.033 \cos \frac{360n}{365} \right) \tau_b \cos \theta_z \tag{10}$$

where  $G_{sc} = 1367 \text{ W m}^{-2}$  is the solar constant,  $n$  is the number of date,  $\tau_b$  is the atmospheric transmittance for beam radiation and  $\theta_z$  is the zenith angle.

Zenith angle is defined as the angle between the incoming beam radiation and the normal on the horizontal surface. Zenith angle is expressed as [41]:

$$\cos \theta_z = \cos \phi \cos \delta \cos \omega + \sin \phi \sin \delta \tag{11}$$

where  $\phi$  is the latitude location of the solar field,  $\delta$  is the declination angle which varies as  $-23.45^\circ \leq \delta \leq 23.45^\circ$  and is given as follows [41]:

$$\delta = 23.45 \sin \left( 360 \frac{284 + n}{365} \right) \tag{12}$$

The hour angle  $\omega$  is a consequence of the rotation on the earth, which spins on its axis at a rate of  $15^\circ$  per hour. The following equation can be considered to calculate the hour angle [41]:

$$\omega = (\text{Hour} - 12) \times 15^\circ \tag{13}$$

The incidence angle for a plane rotated about a horizontal north-south axis with continuous adjustment can be determined from [41]:

$$\cos \theta = \sqrt{\cos^2 \theta_z + \cos^2 \delta \sin^2 \omega} \tag{14}$$

Any collector has a specific incident angle modifier that depends on the incidence angle. For an LS-3 collector, this parameter is calculated by [42]:

$$K(\theta) = 1 - 2.231 \times 10^{-4} \theta - 1.1 \times 10^{-4} \theta^2 + 3.186 \times 10^{-6} \theta^3 + 4.855 \times 10^{-8} \theta^4 \tag{15}$$

Optical efficiency is defined as the ratio of the energy absorbed by the receiver to the energy incident on the collector's aperture. The optical efficiency can be calculated as follows [41]:

$$\eta_{\text{opt}} = \rho_m \alpha_r \tau \gamma \tag{16}$$

where  $\rho_m$  is the reflectance of the mirror,  $\alpha_r$  is the absorptance of the receiver,  $\tau$  is the transmittance of the glass cover and  $\gamma$  is the intercept factor, and their values are given in Table 3 that provides various design parameters of LS-3 collectors.

Row shadowing factor of the PTCs can be expressed as [43]:

$$\eta_{\text{row-shading}} = \frac{L_s \cos \theta_z}{W_a \cos \theta} \tag{17}$$

where  $L_s$  is the distance between two parallel collectors and  $W_a$  is the collector aperture width.

End losses factor which occurs at the end portion of collectors is given by [44]:

$$\eta_{\text{end-loss}} = 1 - \left( 1 + \frac{W_a^2}{48f^2} \right) \left( \frac{f}{L} \right) \tan \theta \tag{18}$$

where  $f$  is the focal length of the collector.



**Table 3** LS-3 collector specification [42]

Parameters	Value
Aperture area/m <sup>2</sup>	545
Aperture width/m	5.76
Length/m	99
Focal length/m	1.71
Mirror reflectivity	0.94
Intercept factor	0.93
Glass transmissivity	0.95
Receiver absorptivity	0.96
Emissivity of glass envelope	0.86
Distance between parallel rows/m	17
Absorber tube inner diameter/m	70
Absorber tube outer diameter/m	54
Glass cover outer diameter/mm	115
Glass cover inner diameter/mm	109
Optical efficiency	0.8
Mirror cleanliness	0.97

Figure 5 shows the schematic of PTCs. The thermal loss coefficient for an LS-3 collector is estimated by an equation given as below [42]:

$$U_L = 2.895475 - 0.0164 (T_{abs} - T_a) + 0.000065 (T_{abs} - T_a)^2 \quad (\text{W/m}^2\text{K}) \quad (19)$$

where  $T_{abs}$  is the absorber temperature.

The overall heat transfer coefficient from the surrounding to inside of the tube is given by [41]:

$$U_o = \left( \frac{1}{U_L} + \frac{D_o}{h_{fi}D_i} + \frac{D_o \ln(D_o/D_i)}{2k} \right)^{-1} \quad (20)$$

where  $D_i$  and  $D_o$  are the inside and outside tube diameters,  $h_{fi}$  is the heat transfer coefficient inside the tube and  $k$  is the thermal conductivity of the tube.

The collector efficiency factor ( $F'$ ) is given as [41]:

$$F' = \frac{U_o}{U_L} \quad (21)$$

The collector flow factor ( $F''$ ) can be calculated by [41]:

$$F'' = \frac{\dot{m} C_p}{A_r U_L F'} \left[ 1 - \exp\left(-\frac{A_r U_L F'}{\dot{m} C_p}\right) \right] \quad (22)$$

where  $\dot{m}$  is the mass flow rate of heat transfer fluid and  $C_p$  is the heat capacity of fluid.

The collector heat removal factor ( $F_R$ (equal to [41]):

$$F_R = F' \times F'' \quad (23)$$

The thermal losses from the pipe ( $Q_{L,pipe}$ ) in the solar field are estimated as [46]:

$$Q_{L,pipe} = (0.01693 \Delta T - 0.000168 \Delta T^2 + 6.78 \times 10^{-7} \Delta T^3) \times A_a \quad (24)$$

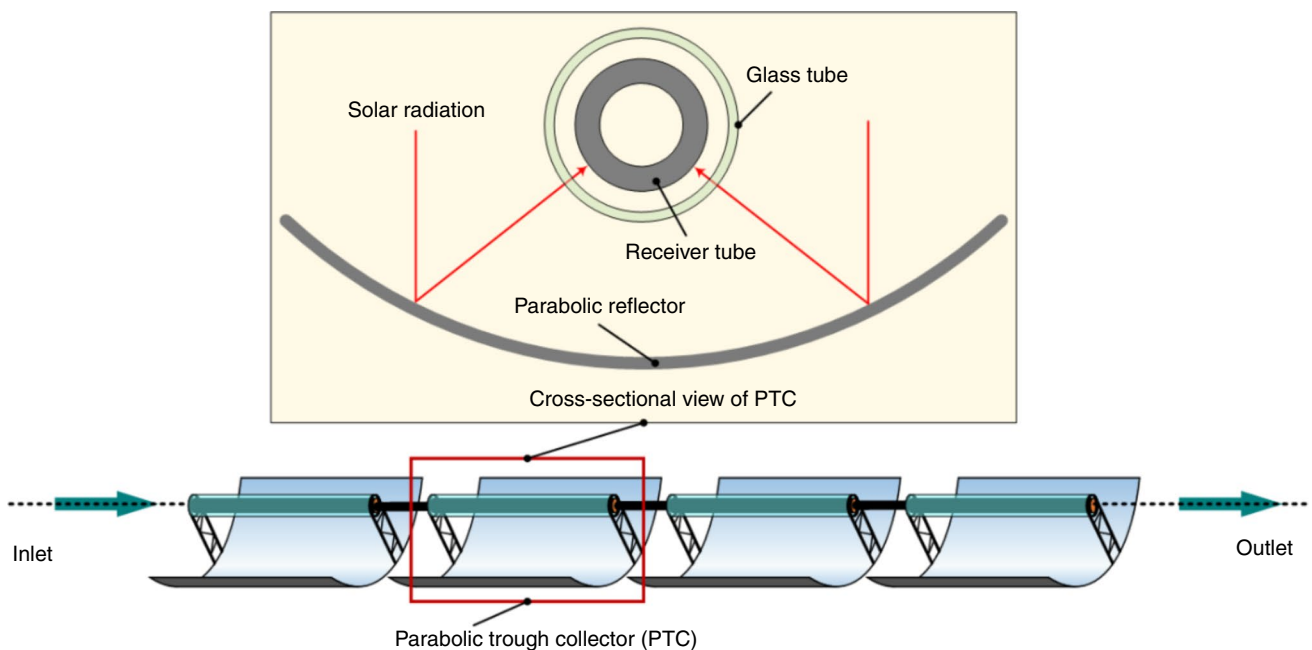


**Fig. 5** Schematic representation of PTC (adopted from [45])

where  $\Delta T$  is the difference between the average field temperature and the ambient temperature.

Part of the solar radiation passing through the Earth’s atmosphere is lost to absorption, reflection and transmitting radiation diffusion. Clouds, mist, dust or even temperature differences among atmospheric layers may be effective. Among these factors, clouds are the most critical factor for radiation losses owing to seasonal changes in cloudiness. In order to obtain the changes, clearness index is defined as the ratio of solar radiation on the horizontal surface to the extraterrestrial radiation at the top layer of the atmosphere. It could be expressed by the following equation [47]:

$$\bar{K}_T = \frac{\bar{H}}{\bar{H}_o} \tag{25}$$

where  $\bar{K}_T$  is the monthly average clearness index,  $\bar{H}$  is the monthly average of daily total radiation received by the horizontal plane on the Earth, and  $\bar{H}_o$  is the radiation received by the same plane outside the Earth’s atmosphere.

The monthly mean of daily extraterrestrial radiation could be estimated for the mean day of the month by using the equation below [41]:

$$H_o = \frac{24 \times 3600}{\pi} G_{sc} \left( 1 + 0.033 \cos \frac{360n}{365} \right) \times \left( \cos \phi \cos \delta \sin \omega_s + \frac{\pi \omega_s}{180} \sin \phi \sin \delta \right) \tag{26}$$

where  $\omega_s$  is the sunset hour angle, in degrees, from the equation:

$$\omega_s = \cos^{-1} (-\tan \phi \tan \delta) \tag{27}$$

If  $G_{sc}$  is in  $W\ m^{-2}$ ,  $H_o$  is in  $J\ m^{-2}$ .

A simple physical-based approach proposed by De Miguel et al. [48] was considered for predicting daily diffuse and direct constituents from daily total solar radiation. According to range of Birjand’s clearness index [47], correlation is expressed by the following equation:

$$\frac{\bar{D}_d}{\bar{H}} = 0.868 + 1.335\bar{K}_T - 5.782\bar{K}_T^2 + 3.721\bar{K}_T^3 \quad (0.13 \leq \bar{K}_T \leq 0.8) \tag{28}$$

$$\bar{B}_d = \bar{H} - \bar{D}_d \tag{29}$$

where  $\bar{D}_d$  is the monthly average of daily diffuse solar radiation and  $\bar{B}_d$  is the monthly average of daily direct solar radiation.

### Supercritical carbon dioxide recompression Brayton cycle

According to previous study [27], the highest energetic efficiency between other Brayton cycles is belonged to the

recompression Brayton cycle. Consequently, the recompression Brayton cycle was chosen for the current study. The proposed SCRBC consists of a main compressor, a recompression compressor, a low-temperature recuperator, a high-temperature recuperator, a turbine, a heat exchanger that gives heat to the water and a precooler rejects the heat to the atmosphere in order that thermodynamic conditions of main compressor are achieved. The split ratio of proposed cycle that flows through precooler is set to  $x$ . Thermodynamic relations (including mass, energy and exergy balance) are derived for all the system’s components, and model of the proposed system is programmed in engineering equation solver (EES). The assumptions considered for this simulation are [49]:

- Steady operating conditions exist in all the system’s components of Brayton cycle.
- Kinetic and potential energy and exergy changes are neglected.
- Pressure losses in the pipes, recuperators and heat exchanger are neglected.
- The turbine and the compressors in the SCRBS have isentropic efficiencies.
- For the recuperators, suitable effectiveness is considered.
- Methane with ambient condition is considered as injected fuel, and chemical reaction in auxiliary boiler is assumed to be complete.

The fluid state at main compressor inlet should be supercritical in order to minimize the compressor work [30]. The design parameters for SCRBC are listed in Table 4.

The main compressor, recompressor and turbine work are modeled based on isentropic efficiency [51] and are defined as:

$$\eta_{comp} = 0.91 - \frac{r_p - 1}{300} \tag{30}$$

**Table 4** Equipment specification of recompression Brayton cycle

Parameters	Value
Compressor inlet temperature/ $^{\circ}C$	31
Compressor inlet pressure/MPa	7.4
Compressor outlet pressure/MPa	20
Compressor isentropic efficiency	0.9
Low-temperature recuperator effectiveness [50]	0.7
High-temperature recuperator effectiveness [50]	0.85
Turbine isentropic efficiency	0.89
Turbine inlet temperature/ $^{\circ}C$	650
Split ratio	0.625
Carbon dioxide mass flow rate/kg $s^{-1}$	26.5

$$W_{\text{comp}} = x \dot{m}_{\text{CO}_2} \left( \frac{h_{\text{out,s}} - h_{\text{in}}}{\eta_{\text{comp}}} \right) \tag{31}$$

$$W_{\text{Recomp}} = (1 - x) \dot{m}_{\text{CO}_2} \left( \frac{h_{\text{out,s}} - h_{\text{in}}}{\eta_{\text{comp}}} \right) \tag{32}$$

$$\eta_{\text{tur}} = 0.9 - \frac{r_p - 1}{250} \tag{33}$$

$$W_{\text{tur}} = \dot{m}_{\text{CO}_2} \eta_{\text{tur}} (h_{\text{in}} - h_{\text{out,s}}) \tag{34}$$

where  $r_p$  is the pressure ratio for compressors and turbine, which are equal.

The recuperators model is based on the definition of effectiveness [52]. The effectiveness of the low-temperature recuperator is defined as follows:

$$\varepsilon_{\text{LTR}} = \frac{q_{\text{real}}}{q_{\text{max}}} = \frac{h_3 - h_2}{h_8 - h_2} \tag{35}$$

Also, the effectiveness of the high-temperature recuperator is defined as:

$$\varepsilon_{\text{HTR}} = \frac{q_{\text{real}}}{q_{\text{max}}} = \frac{h_5 - h_4}{h_7 - h_4} \tag{36}$$

The first law of thermodynamics in the low-temperature recuperator can be formulated as:

$$x (h_3 - h_2) = h_8 - h_9 \tag{37}$$

The first law of thermodynamics in the high-temperature recuperator can be formulated as:

$$h_5 - h_4 = h_7 - h_8 \tag{38}$$

The heat added by the auxiliary boiler is calculated by:

$$Q_{\text{AuxB}} = \dot{m}_{\text{CO}_2} (h_6 - h_{\text{SR}_0}) \tag{39}$$

Thermodynamic relations for the heat exchanger are given by:

$$\dot{m}_{\text{CO}_2} (h_9 - h_{11}) = \dot{m}_w (h_{14} - h_{13}) \tag{40}$$

The energy rejected at the precooler is given by:

$$Q_{\text{out}} = x \dot{m}_{\text{CO}_2} (h_{11} - h_1) \tag{41}$$

Finally, the thermal efficiency of the cycle is calculated by:

$$\eta_{\text{th}} = \frac{W_{\text{tur}} - W_{\text{comp}} - W_{\text{Recomp}}}{Q_u + Q_{\text{AuxB}}} \tag{42}$$

In order to validate the proposed mathematical modeling, it was necessary to compare the results of the present study with similar reliable studies in the literature. Based on the proposed system, two benchmarks (solar fields and SCRBC) should be defined. For solar fields, all the simulation equations were adopted from [41] and were applied to Birjand as the case study. For the supercritical carbon dioxide recompression Brayton cycle, the results were compared with previous literatures [53, 54]. It should be noted that all of the modeling conditions and assumptions are assumed to be same between the present study and reference studies. The condition setting and results comparison are presented in Table 3. By comparing the results, it can be stated the relative difference for thermal efficiency is 2.95% and 1.47% when the results of the present study are compared with Turchi's study [53] and Cheng's study [54], respectively. It shows that the calculated thermal efficiency for same turbine inlet temperature is in excellent agreement with the previous studies in the field (Table 5).

**Table 5** Condition setting and results comparison of thermal efficiency

Parameters			Value
Minimum temperature/°C			32
Minimum pressure/MPa			7.38
Pressure ratio			3.4
Compressor isentropic efficiency			0.89
Low- and high-temperature recuperator effectiveness			0.95
Turbine inlet temperature/°C			550
Turbine isentropic efficiency			0.93
<i>Thermal efficiency</i>	Turchi's study/% [53]	Cheng's study/% [54]	The present study/%
	40.4	39.82	39.24

### Exergy analysis of the system

Exergy is the maximum useful work that could be obtained from the system at a given state in a specified environment. The second law of thermodynamics handles the quality of energy. However, the first law handles the quantity of energy [55]. In order to irreversibility, which is wasted work potential during a process, the exergy is always destroyed. The exergy balance equation for a steady flow process can be expressed as follows:

$$\dot{E}_Q - \dot{E}_W + \sum \dot{m} \psi_{in} - \sum \dot{m} \psi_{out} - \dot{E}_d = 0 \tag{43}$$

in which  $\dot{E}_Q$  is the rate of the exergy transfer by heat,  $\dot{E}_W$  is the rate of the exergy transfer by work,  $\psi$  is the flow exergy and  $\dot{E}_d$  is the rate of the exergy destruction.

The total solar exergy input to the system can be expressed as [50]:

$$\dot{E}_{in,s} = A_a G_b \left( 1 - \frac{4 T_0}{3 T_s} + \frac{1}{3} \left( \frac{T_0}{T_s} \right)^4 \right) \tag{44}$$

where  $T_s$  is the sun’s outer surface temperature that is considered 5777 K and  $T_0$  is the ambient temperature.

In order to calculate the inlet exergy of fuel, only its chemical exergy is considered and can be written as the following equation:

$$\dot{E}_{in,f} = \dot{m}_f e^{ch} \tag{45}$$

where  $e^{ch}$  is the specific chemical exergy of methane as injected fuel in auxiliary boiler.

The exergy efficiency (the second-law efficiency) is defined as the ratio of the exergy recovered to the exergy expended [55], which is expressed by the following equation:

$$\eta_{ex} = \frac{\dot{E}_{out}}{\dot{E}_{in}} = \frac{\dot{W}_{net}}{\dot{E}_{in,s} + \dot{E}_{in,f}} \tag{46}$$

According to above equations, the exergy equation for each of the system components is summarized in Table 6.

### Economic analysis

For the economic analysis of the proposed system, two approaches have been carried out. Firstly, the payback period and then the net present value (NPV) are calculated and investigated. These methods are used to assess the investment of the project and decide to accept or reject it. The payback period could be calculated as below [10]:

$$\text{Payback period} = \frac{\text{Initial investment}}{\text{Net annual cash inflows}} \tag{47}$$

The equipment costs are needed for calculating the initial investment of the plant. The correlations of purchased equipment cost for the system components are given in Table 7. Also, the total investment cost of LS-3 collectors (including the heat collection elements, installation, piping, mirrors, etc.) is assumed 355 \$ per square meter of aperture area. The proposed system has two valuable profit factors. The first one is saving fuel, and another one is power generation. According to universal NG price, the fuel cost is considered 0.31 \$ m<sup>-3</sup> and the expected yearly sales of electricity are assumed 0.14 \$ kWh<sup>-1</sup>.

As the PBR method doesn’t consist of the inflation rate and some important economic factors, the NPV is used as a better approach for economic assessment. The NPV can be calculated as:

$$\text{NPV} = \sum_{t=1}^N \frac{R_t}{(1 + i)^t} \tag{48}$$

**Table 6** Exergy equation for each of the system components

Component	Equations
Compressor	$\dot{W}_{comp} + \dot{m}_1 \psi_1 - \dot{m}_2 \psi_2 - \dot{E}_{d,comp} = 0$
Recompressor	$\dot{W}_{Recomp} + \dot{m}_9 \psi_9 - \dot{m}_{10} \psi_{10} - \dot{E}_{d,Recomp} = 0$
Turbine	$-\dot{W}_{tur} + \dot{m}_6 \psi_6 - \dot{m}_7 \psi_7 - \dot{E}_{d,tur} = 0$
Low-temperature recuperator	$\dot{m}_2 \psi_2 + \dot{m}_8 \psi_8 - \dot{m}_3 \psi_3 - \dot{m}_9 \psi_9 - \dot{E}_{d,LTR} = 0$
High-temperature recuperator	$\dot{m}_4 \psi_4 + \dot{m}_7 \psi_7 - \dot{m}_5 \psi_5 - \dot{m}_8 \psi_8 - \dot{E}_{d,HTR} = 0$
Precooler	$-\dot{E}_{Pc} + \dot{m}_{11} \psi_{11} - \dot{m}_1 \psi_1 - \dot{E}_{d,Pc} = 0$
Solar receiver	$\dot{E}_{in,s} + \dot{m}_{SR_i} \psi_{SR_i} - \dot{m}_{SR_o} \psi_{SR_o} - \dot{E}_{d,SR} = 0$
Auxiliary boiler	$\dot{E}_{in,AuxB} + \dot{m}_{SR_o} \psi_{SR_o} - \dot{m}_6 \psi_6 - \dot{E}_{d,AuxB} = 0$
Heat exchanger	$\dot{m}_9 \psi_9 + \dot{m}_{13} \psi_{13} - \dot{m}_{11} \psi_{11} - \dot{m}_{14} \psi_{14} - \dot{E}_{d,HE} = 0$
CGS heater	$\dot{m}_{14} \psi_{14} + \dot{m}_{NG_1} \psi_{NG_1} - \dot{m}_{12} \psi_{12} - \dot{m}_{NG_2} \psi_{NG_2} - \dot{E}_{d,CGS} = 0$
Throttling valve	$\dot{m}_{NG_2} \psi_{NG_2} - \dot{m}_{NG_3} \psi_{NG_3} - \dot{E}_{d,TV} = 0$

**Table 7** Correlations of purchased equipment cost [56]

Component	Purchased equipment cost	Year	CI <sub>new</sub> /CI <sub>ref</sub>
Compressor	$PEC_{comp} = \frac{71.10\dot{m}_{CO_2}}{0.9-\eta_{comp}} \left( \frac{P_{out}}{P_{in}} \right) \ln \left( \frac{P_{out}}{P_{in}} \right)$	1995	1.61
Turbine	$PEC_{tur} = \frac{479.34\dot{m}_{CO_2}}{0.92-\eta_{tur}} \left( \frac{P_{in}}{P_{out}} \right) [1 + \exp(0.036 T_{in} - 54.4)]$	1995	1.61
Auxiliary boiler	$PEC_{aux.B} = \frac{46.08\dot{m}_{CO_2}}{(0.995-\frac{P_4}{P_3})} [1 + \exp(0.018 T_4 - 26.4)]$	1995	1.61
Recuperator	$PEC_{rec} = 4122 \times \left( \frac{\dot{m}_{CO_2}(h_5-h_6)}{18 \times \Delta TLM} \right)^{0.6}$	1995	1.61
Heat exchanger	$PEC_{HE} = 190 + 310 \times A_{HE}$	2010	1.13

where *t* is the number of time periods, *i* is a discount rate that could be earned in alternative investment and *R<sub>t</sub>* is net cash inflow–outflows during a single period. It should be noticed that the discount rate for USD is considered 15%.

For converting the purchasing cost of equipment from the base year to the reference year, cost index is employed as below:

$$PEC_{new} = PEC_{ref} \times \frac{CI_{new}}{CI_{ref}} \tag{49}$$

where CI is the cost index. The values of the cost index are adapted from Marshall and Swift cost index.

## Results and discussion

### Current CGS information

The information related to the temperature of the NG and the ambient temperature is the most critical parameters for determining the working conditions of the system. The significance of the ambient temperature can be found in determining the temperature of the soil and estimating the temperature of the gas due to Eq. (3) discussed in the preceding sections. Figure 6 shows the daily average temperature changes over the whole year per each month for NG and the environment. According to the expectation, the temperature in the cold months of the year, such as December or February, reaches its lowest possible amount, and hence, the maximum thermal energy is required. Accordingly, the parameters required to design the proposed system are selected based on these conditions.

Figure 7 shows variations in the average daily inlet pressure in the Birjand NG station in terms of months of the year. According to the diagram, the highest inlet pressure is recorded for the cold months of the year, which is important for determining the hydrate temperature of the NG and the optimal NG outlet temperature can be estimated in accordance with it (which is considered to be 10 °C in this

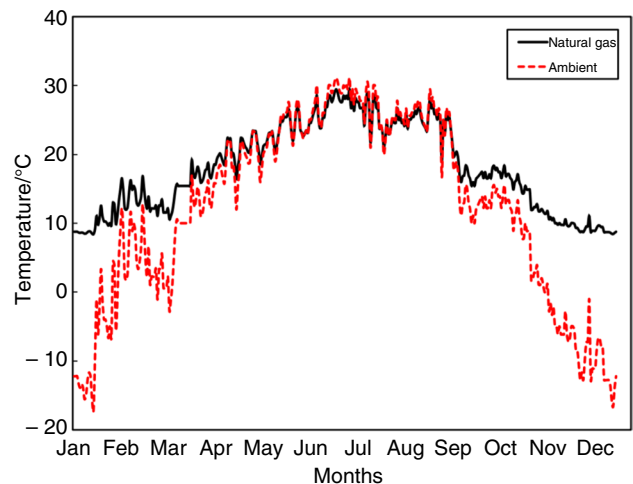


**Fig. 6** Inlet natural gas and ambient temperatures of Birjand CGS in 2019

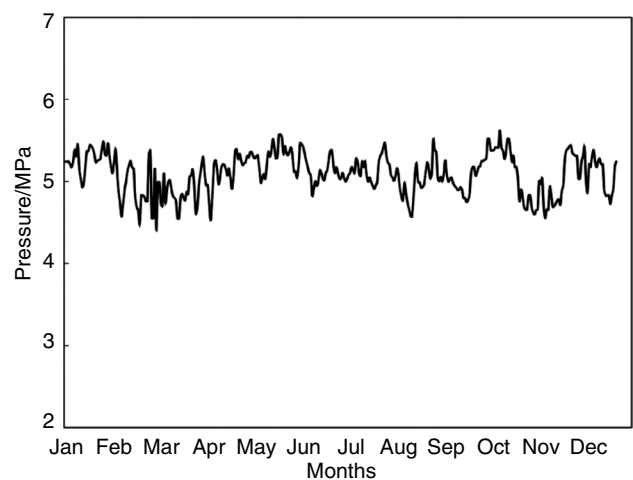


**Fig. 7** Inlet natural gas pressure of Birjand CGS in 2019

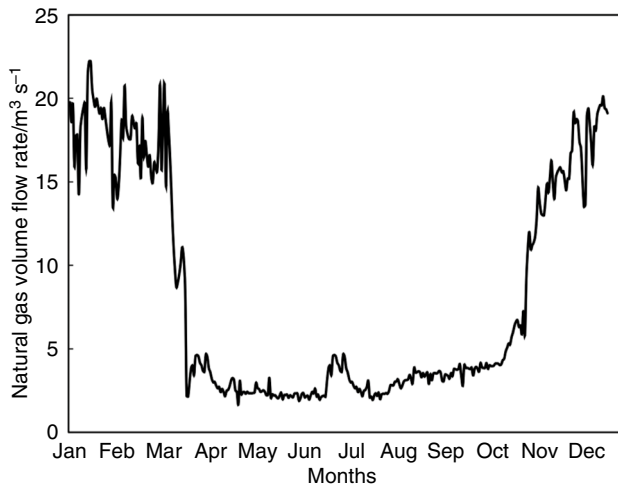


**Fig. 8** Natural gas volume flow rate of Birjand CGS over a whole year

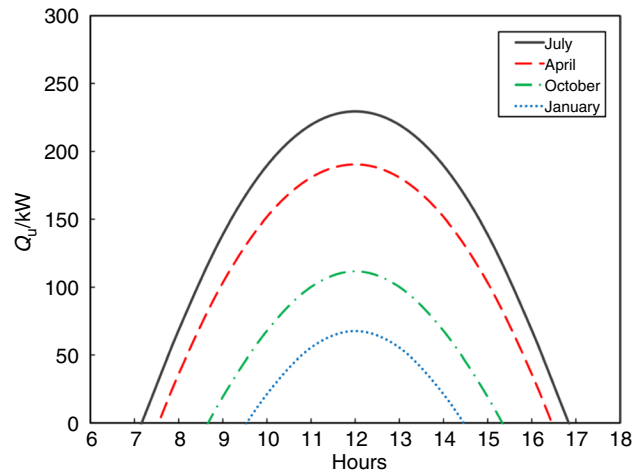


**Fig. 10** Useful energy for the average day of month

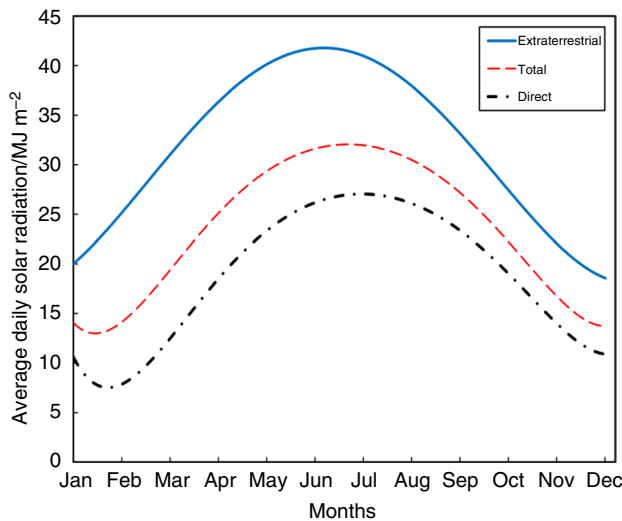


**Fig. 9** Extraterrestrial, total and direct average daily solar radiation over a whole year of Birjand

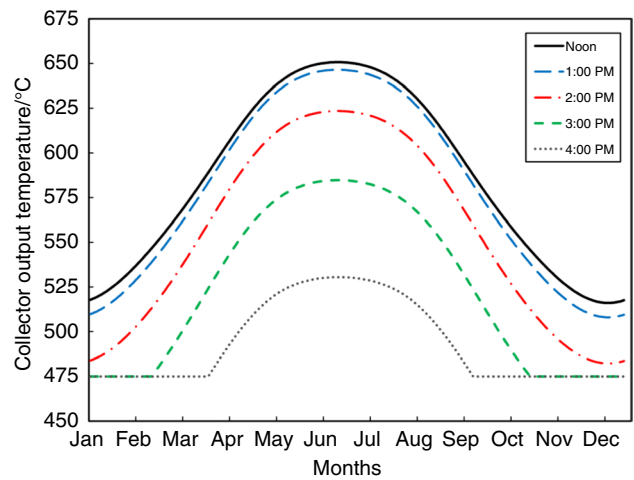


**Fig. 11** Outlet temperature of LS-3 collectors for all a year

proposed system). It's worth mentioning that the outlet pressure of NG is fixed at 1.72 MPa.

The daily volume flow rate diagram of the Birjand CGS throughout the year is plotted in Fig. 8. According to this chart, the maximum amount of volume flow rate passes through the station in winter, reaching about  $22 \text{ m}^3 \text{ s}^{-1}$  in February.

It should be pointed out that all data presented in this section are collected by the local natural gas company.

**Available solar energy**

Figure 9 demonstrates the average daily solar energy outside the atmosphere, the total energy passing through the

atmosphere and the direct energy received by collectors for the Birjand CGS. As mentioned, not all solar energy outside the atmosphere reaches the earth surface and a part of it disappears, in which the clearness index shows the ratio of the energy received by the earth surface. Given that total solar energy consists of two parts: direct and diffuse energy, it can be noted that the difference between total energy and direct energy is equal to the energy diffuse at the earth's surface, in which this difference reaches its highest amount between February and March.

Figure 10 illustrates the amount of solar energy absorbed by collectors for the average day of 1 month of each season. As expected, the highest amount of the absorbed energy is for July (in summer) with the longest day and the lowest one is for January (in winter) with the shortest day length.

Figure 11 shows the temperature distribution of the collector output for all the months of the year at five different

**Table 8** Thermodynamic state of proposed system

State	$T/^\circ\text{C}$	$P/\text{MPa}$	$h/\text{kJ kg}^{-1}$	$s/\text{kJ kg}^{-1} \text{K}^{-1}$
1	31	7.4	-184.5	-1.338
2	68.05	20	-161.8	-1.332
3	156.4	20	26.74	-0.8351
4	163	20	37.05	-0.8113
5	475.6	20	436.5	-0.1149
6	650	20	653.3	0.1453
7	523.7	7.4	507	0.1675
8	175.6	7.4	107.5	-0.4894
9	79.17	7.4	-10.29	-0.7863
10	174.3	20	54.23	-0.7724
11	44.22	7.4	-72.23	-0.9723
12	30.97	0.3	130	0.4498
13	31	1.5	131.2	0.4498
14	60	1.5	252.4	0.8304
NG <sub>1</sub>	8.4	5.9	-104	-2.408
NG <sub>2</sub>	27.58	5.9	-52.7	-2.232
NG <sub>3</sub>	10	1.8	-52.7	-1.655

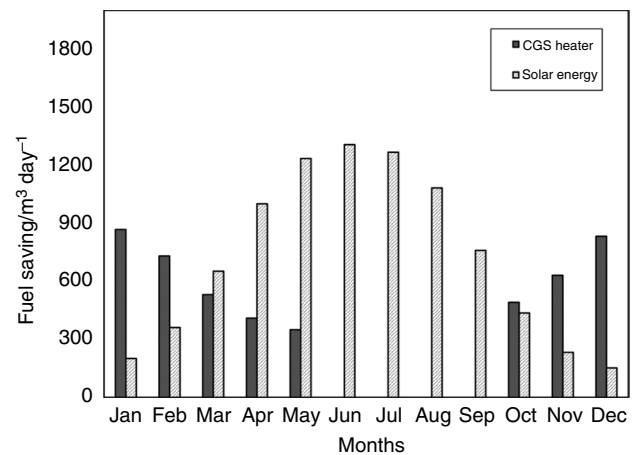
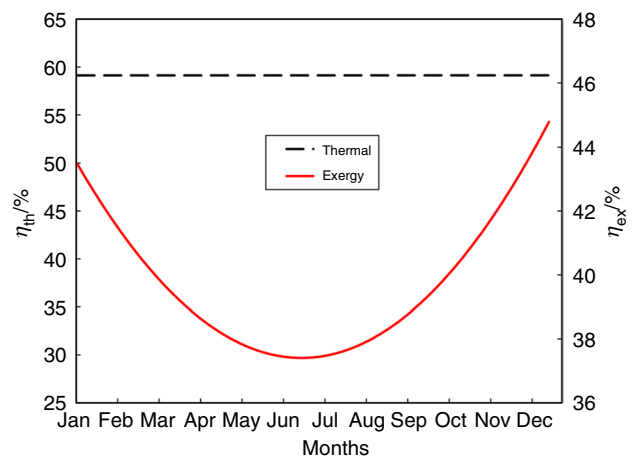
**Table 9** Result of simulation for the proposed system

Parameters	Value
Turbine power/kW	3880
Main compressor power/kW	377
Recompression compressor power/kW	641
Heat rejection/kW	1860
Average heat absorption from solar collector/kW	415
Number of collector rows	25
Average thermal efficiency/%	56
Average exergy efficiency/%	41
Net power output/kW	2862
Carbon dioxide mass flow rate/kg s <sup>-1</sup>	26.5

times. As expected, the outlet temperature reaches to its maximum amount at noon for all days. The value of the selected flow rate for each row of collectors is selected so that the maximum output temperature throughout the year (which occurs between June and July) does not exceed the maximum operating temperature of the proposed cycle (650 °C).

### Proposed system

In the present study, the proposed system (Fig. 3) is simulated to validate the feasibility of preheating natural gas with a heat rejection of a solar SCRBC. The thermodynamic states for each stream of the proposed system are summarized in Table 8, and Table 9 presents some outputs of the simulation procedure.

**Fig. 12** Fuel saving of the proposed system over a whole year**Fig. 13** Thermal and exergy efficiency of system over a whole year

The use of the heat rejection from the cycle for preheating of natural gas in the CGS causes the NG that utilized for this duty is saved, and furthermore, environmental pollution is reduced. As shown in Fig. 12, in the warmer months of the year (from June to September), there is no need to preheat natural gas and the consumption of NG as fuel is zero at this time. Also, employing solar energy during the day reduces fuel consumption of heat source in order to generate electricity. As shown in Fig. 12, the highest reduction in occurs in June. Figure 12 shows a comparison between the fuel saving in CGS heater and reduction in fuel consumption due to the applying solar energy in the current system over a whole year. The total amount of fuel saving for proposed system is estimated at 4.87 million cubic meters annually.

The thermal and exergy efficiency of the suggested cycle over a whole year is depicted in Fig. 13. By keeping the gas turbine inlet temperature as a constant value, an auxiliary boiler is required to bring the carbon dioxide temperature

to the required temperature. This auxiliary boiler has the task of providing the required heat load during the day as well as at night when solar power is not available. Due to the constant maximum temperature of the cycle, the thermal efficiency remains constant throughout the year. However, the exergy efficiency will not be uniform and has the highest value in the month of December while the lowest value is occurred in June. The reason of this phenomenon could be found in the sever exergy destruction due to the most heat loss in solar collectors in the warmer months of the year compared to the colder one.

As the values are comparable, the exergy destruction of all the system components is plotted in Fig. 14. This figure shows the contribution of each system component in the total exergy destruction. Analyzing the results indicates that the highest exergy destruction occurred in throttling valve and the solar collectors have the second highest exergy destruction. Due to the drastic drop pressure and hence the severe temperature difference, the most exergy destruction belongs to throttling valve among all other system components. Additionally, for this case that the direct normal irradiation is high, there is a major difference between the absorber temperature and the ambient temperature. As a result, the auxiliary boiler has lower exergy destruction as compared to the exergy destruction of solar collectors. According to the exergy destruction analysis, replacing the throttling valve by a turbo expander and an electricity generator can decrease the exergy destruction rate during the pressure reduction process as well as produce power [25]. Moreover, employing a thermal energy storage in solar fields can reduce exergy destruction of solar collectors and provide heat demand during nighttime.

Fig. 14 Exergy destruction analysis of the system

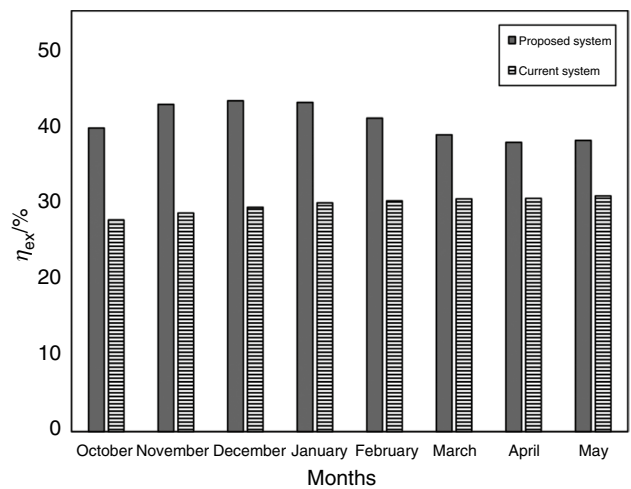
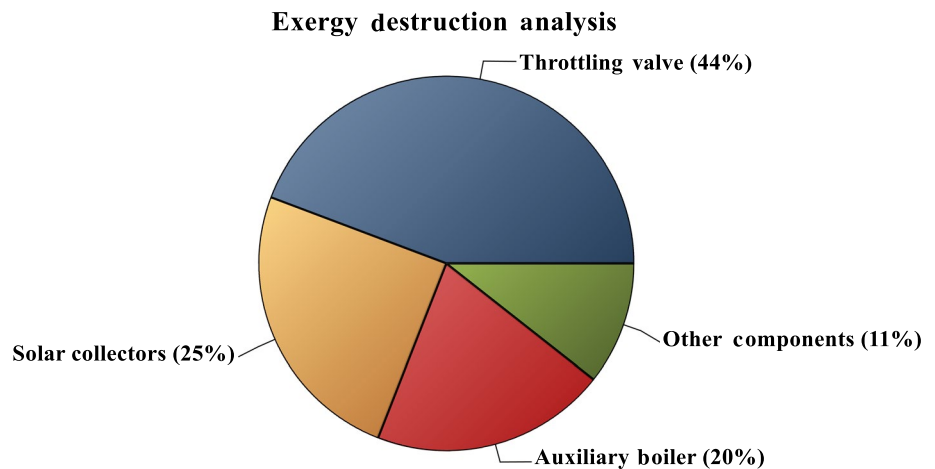


Fig. 15 Comparison between exergy efficiency of the CGS in current system and proposed one

Figure 15 shows the exergy efficiency of the proposed system and the current heaters for preheating the NG in Birjand CGS. As it is demonstrated, the exergy efficiency of the suggested system is more than the current one for those months of the year which natural gas preheating is required. According to results, the average annual exergy efficiency of the proposed system and current one is 41% and 29%, respectively. The higher efficiency indicates the superiority of the suggested system over utilize of the current heaters in the CGS. Also, the exergy destruction of the throttling valve by using heaters in the CGS is 68%, while this value in the proposed system is 44%.



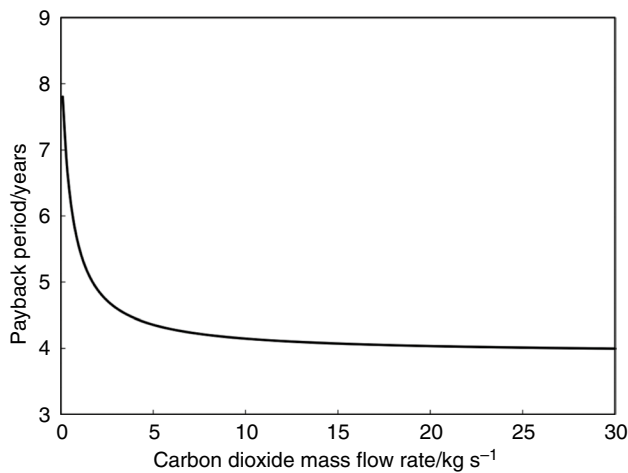


Fig. 16 Effect of carbon dioxide mass flow rate on payback period

**Economic analysis**

The optimal choice of carbon dioxide mass flow rate is carried out based on the economic cost and size of the Brayton cycle. The carbon dioxide mass flow rate diagram is plotted in Fig. 15 on the basis of the payback period. According to this figure, with the increase in the mass flow rate, the return period of capital has remained almost constant and is approaching 4 years. Considering the required surface area for heat transfer and installation of solar collectors and also taking into account Fig. 16, the optimum carbon dioxide mass flow rate of 26.5 kg s<sup>-1</sup> is chosen for the

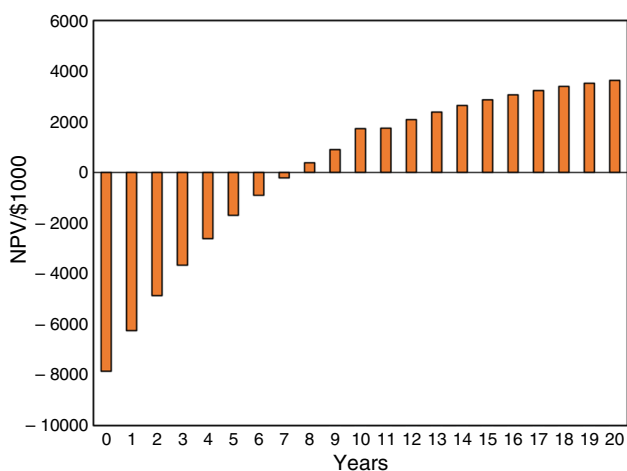


Fig. 17 NPV analysis of the proposed system in 20 years

proposed recompression Brayton cycle. According to this value, 25 collector rows and the payback period of 4 years are obtained. The payback period for the proposed cycle integrated with solar energy as high-temperature source of it is about 4 years, while this parameter for the other systems that utilize solar collector with and without storage tank to preheat natural gas directly is roughly 6 and 9 years, respectively [8, 10].

Another important economic factor is the analysis of the net present value (NPV), which is depicted in Fig. 17. This factor provides a more accurate and powerful criteria for the economic evaluation of the proposed system by taking into account the discount rate for the project. Based on the NPV analysis, it takes 8 years from the exploitation of the project to achieve a positive profit of 380 thousand dollars. According to the figure, at the end of the 20th year, the NPV reaches near 3.6 million dollars.

Finally, the sensitivity analysis for the project is drawn in Fig. 18. This figure is investigated in 3 different situations. In the first case, only changes in the rate of the produced electricity relative to the base price (0.14 \$ kWh<sup>-1</sup>) are assumed, which is the negative gradient of the graph showing a decrease in the payback period with the increase in the base price. In the latter case, the impact of NG prices is studied, which results in a longer payback period with an increase in base prices (0.31 \$ m<sup>-3</sup>). In the last case, the change in both factors is considered simultaneously. As it could be realized, the payback period is reduced with increasing the base prices and the figure indicates that it approaches 2 years, which is a positive feature of the project.

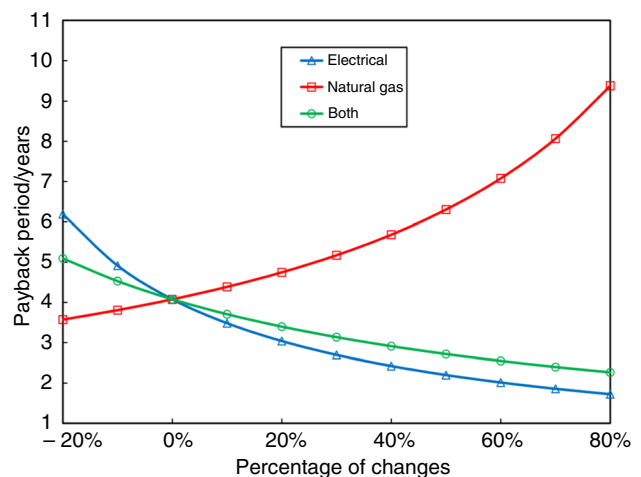


Fig. 18 Sensitive analysis of Payback period for the proposed system

## Conclusions

Natural gas must be warmed up in a city gate station before pressure reduction takes place. In this study, a supercritical carbon dioxide recompression Brayton cycle integrated with solar energy was proposed to be employed in a CGS to provide the required heat for preheating the natural gas and generate electricity simultaneously. For the first time in this field, heat rejection from an SCRBC equipped with solar energy was recovered to preheat the natural gas. The proposed configuration was employed in the Birjand CGS as a case study and a comprehensive techno-economic analysis carried out to evaluate its performance. The following can be concluded from this study:

1. The proposed power cycle employs an LS-3 parabolic trough collectors with 25 rows and an auxiliary boiler for providing heat input. Adding an auxiliary boiler into the solar system will make the power output uniform. The total amount of fuel saving is estimated at 4.87 million cubic meters annually, and the net power generation is equal to 2.86 MW.
2. The results showed that the annual average of thermal and exergy efficiency is 0.56 and 0.41, respectively. The results of the exergy analysis demonstrate that the most exergy destruction occurred in throttling valve and after that took place in the solar collectors and auxiliary boiler, respectively.
3. The economic analysis indicates that the payback period for the proposed system is 4 years. Based on the NPV method, as a more accurate economic evaluation, it takes 8 years to return all the total investment, and at the end of this year, the positive profit 380 thousand dollars could be achieved.

**Acknowledgements** This work has been supported by Birjand Gas Co., and the authors would like to thank this company for their technical and financial support.

## References

1. Mehrpooya M, Ghorbani B. Introducing a hybrid oxy-fuel power generation and natural gas/carbon dioxide liquefaction process with thermodynamic and economic analysis. *J Clean Prod.* 2018;204:1016–33.
2. Weijermars R. Guidelines for clockspeed acceleration in the US natural gas transmission industry. *Appl Energy.* 2010;87(8):2455–66.
3. Farzaneh-Gord M, Hashemi S, Sadi M. Energy destruction in Iran's natural gas pipe line network. *Energy Explor Exploit.* 2007;25(6):393–406.
4. Ghorbani B, Mehrpooya M, Ghasemzadeh H. Investigation of a hybrid water desalination, oxy-fuel power generation and CO<sub>2</sub> liquefaction process. *Energy.* 2018;158:1105–19.
5. Farzaneh-Gord M, Maghrebi MJ. Exergy of natural gas flow in Iran's natural gas fields. *Int J Exergy.* 2009;6(1):131–42.
6. Rahmati A, Reiszadeh M. An experimental study on the effects of the use of multi-walled carbon nanotubes in ethylene glycol/water-based fluid with indirect heaters in gas pressure reducing stations. *Appl Therm Eng.* 2018;134:107–17.
7. Naderi M, Ahmadi G, Zarringhalam M, Akbari O, Khalili E. Application of water reheating system for waste heat recovery in NG pressure reduction stations, with experimental verification. *Energy.* 2018;162:1183–92.
8. Farzaneh-Gord M, Arabkoohsar A, Rezaei M, Deymi-Dashtebayaz M, Rahbari H. Feasibility of employing solar energy in natural gas pressure drop stations. *J Energy Inst.* 2011;84(3):165–73.
9. Farzaneh-Gord M, Arabkoohsar A, Dasht-bayaz MD, Farzaneh-Kord V. Feasibility of accompanying uncontrolled linear heater with solar system in natural gas pressure drop stations. *Energy.* 2012;41(1):420–8.
10. Farzaneh-Gord M, Arabkoohsar A, Dasht-bayaz MD, Machado L, Koury R. Energy and exergy analysis of natural gas pressure reduction points equipped with solar heat and controllable heaters. *Renew Energy.* 2014;72:258–70.
11. Farzaneh-Gord M, Ghezelbash R, Arabkoohsar A, Pilevari L, Machado L, Koury R. Employing geothermal heat exchanger in natural gas pressure drop station in order to decrease fuel consumption. *Energy.* 2015;83:164–76.
12. Farzaneh-Gord M, Sadi M. Enhancing energy output in Iran's natural gas pressure drop stations by cogeneration. *J Energy Inst.* 2008;81(4):191–6.
13. Borelli D, Devia F, Cascio EL, Schenone C. Energy recovery from natural gas pressure reduction stations: integration with low temperature heat sources. *Energy Convers Manag.* 2018;159:274–83.
14. Xiong Y, An S, Xu P, Ding Y, Li C, Zhang Q, et al. A novel expander-depending natural gas pressure regulation configuration: performance analysis. *Appl Energy.* 2018;220:21–35.
15. Olfati M, Bahiraei M, Heidari S, Veysi F. A comprehensive analysis of energy and exergy characteristics for a natural gas city gate station considering seasonal variations. *Energy.* 2018;155:721–33.
16. Olfati M, Bahiraei M, Veysi F. A novel modification on preheating process of natural gas in pressure reduction stations to improve energy consumption, exergy destruction and CO<sub>2</sub> emission: preheating based on real demand. *Energy.* 2019;173:598–609.
17. Ashouri E, Veisy F, Asadi M, Azizpour H, Sadr A. Influence of tube arrangement on the thermal performance of indirect water bath heaters. *J Chem Pet Eng.* 2013;47(2):69–81.
18. Salari S, Goudarzi K. Heat transfer enhancement and fuel consumption reduction in heaters of CGS gas stations. *Case Stud Therm Eng.* 2017;10:641–9.
19. Salari S, Goudarzi K. Intensification of heat transfer in heater tubes of city gas stations using spiral spring inserts. *Therm Sci Eng Prog.* 2017;3:123–32.
20. Khosravi M, Arabkoohsar A, Alsagri AS, Sheikholeslami M. Improving thermal performance of water bath heaters in natural gas pressure drop stations. *Appl Therm Eng.* 2019;159:113829.
21. Mehrpooya M, Ghorbani B, Hosseini SS. Developing and exergetic performance assessment of biogas upgrading process driven by flat plate solar collectors coupled with Kalina power cycle. *Energy Convers Manag.* 2019;181:398–413.
22. Qiu Y, Li M-J, He Y-L, Tao W-Q. Thermal performance analysis of a parabolic trough solar collector using supercritical CO<sub>2</sub> as heat transfer fluid under non-uniform solar flux. *Appl Therm Eng.* 2017;115:1255–65.

23. Bellos E, Tzivanidis C. Parametric investigation of supercritical carbon dioxide utilization in parabolic trough collectors. *Appl Therm Eng.* 2017;127:736–47.
24. Wang J, Wang J, Lund PD, Zhu H. Thermal performance analysis of a direct-heated recompression supercritical carbon dioxide Brayton cycle using solar concentrators. *Energies.* 2019;12(22):4358.
25. Arabkoohsar A, Farzaneh-Gord M, Deymi-Dashtebayaz M, Machado L, Koury R. A new design for natural gas pressure reduction points by employing a turbo expander and a solar heating set. *Renew Energy.* 2015;81:239–50.
26. Renewable energy organization of Iran website. <http://www.satba.gov.ir/>. 2019.
27. Al-Sulaiman FA, Atif M. Performance comparison of different supercritical carbon dioxide Brayton cycles integrated with a solar power tower. *Energy.* 2015;82:61–71.
28. Ahn Y, Bae SJ, Kim M, Cho SK, Baik S, Lee JI, et al. Review of supercritical CO<sub>2</sub> power cycle technology and current status of research and development. *Nucl Eng Technol.* 2015;47(6):647–61.
29. Padilla RV, Too YCS, Benito R, Stein W. Exergetic analysis of supercritical CO<sub>2</sub> Brayton cycles integrated with solar central receivers. *Appl Energy.* 2015;148:348–65.
30. Coco-Enrriquez L, Muñoz-Antón J, Martínez-Val J. New text comparison between CO<sub>2</sub> and other supercritical working fluids (ethane, Xe, CH<sub>4</sub> and N<sub>2</sub>) in line-focusing solar power plants coupled to supercritical Brayton power cycles. *Int J Hydrog Energy.* 2017;42(28):17611–31.
31. Sharan P, Neises T, McTigue JD, Turchi C. Cogeneration using multi-effect distillation and a solar-powered supercritical carbon dioxide Brayton cycle. *Desalination.* 2019;459:20–33.
32. Gkountas AA, Stamatelos AM, Kalfas AI, editors. Thermodynamic modeling and comparative analysis of supercritical carbon dioxide Brayton cycle. ASME Turbo Expo 2017: Turbomachinery technical conference and exposition; 2017: American Society of Mechanical Engineers Digital Collection.
33. Fernández-García A, Zarza E, Valenzuela L, Pérez M. Parabolic-trough solar collectors and their applications. *Renew Sustain Energy Rev.* 2010;14(7):1695–721.
34. Khan J, Arsalan MH. Solar power technologies for sustainable electricity generation—a review. *Renew Sustain Energy Rev.* 2016;55:414–25.
35. Arnold K, Stewart M. Surface production operations, volume 2: design of gas-handling systems and facilities. Amsterdam: Elsevier; 1999.
36. Edalat M, Mansoori GA. Buried gas transmission pipelines: temperature profile prediction through the corresponding states principle. *Energy Sources.* 1988;10(4):247–52.
37. Najafimoud M, Alizadeh A, Mohamadian A, Mousavi J. Investigation of relationship between air and soil temperature at different depths and estimation of the freezing depth (case study: Khorasan Razavi). 2008.
38. Bergman TL, Incropera FP, DeWitt DP, Lavine AS. Fundamentals of heat and mass transfer. New York: Wiley; 2011.
39. Kalogirou SA. Solar energy engineering: processes and systems. 2nd ed. Amsterdam: Academic Press; 2013.
40. Zhou L, Li Y, Hu E, Qin J, Yang Y. Comparison in net solar efficiency between the use of concentrating and non-concentrating solar collectors in solar aided power generation systems. *Appl Therm Eng.* 2015;75:685–91.
41. Duffie JA, Beckman WA. Solar engineering of thermal processes. New York: Wiley; 2013.
42. Goswami DY, Kreith F. Energy efficiency and renewable energy handbook. Boca Raton: CRC Press; 2015.
43. Stuetzle T. Automatic control of the 30MWe SEGS VI parabolic trough plant. Master Thesis, University of Wisconsin-Madison, College of Engineering. 2002.
44. Qin J, Hu E, Nathan GJ. The performance of a solar aided power generation plant with diverse “configuration-operation” combinations. *Energy Convers Manag.* 2016;124:155–67.
45. Li L, Sun J, Li Y, He Y-L, Xu H. Transient characteristics of a parabolic trough direct-steam-generation process. *Renew Energy.* 2019;135:800–10.
46. Patnode AM. Simulation and performance evaluation of parabolic trough solar power plants. Madison: University of Wisconsin; 2006.
47. Alamdari P, Nematollahi O, Alemrajabi AA. Solar energy potentials in Iran: a review. *Renew Sustain Energy Rev.* 2013;21:778–88.
48. De Miguel A, Bilbao J, Aguiar R, Kambezidis H, Negro E. Diffuse solar irradiation model evaluation in the north Mediterranean belt area. *Sol Energy.* 2001;70(2):143–53.
49. Zare V, Hasanzadeh M. Energy and exergy analysis of a closed Brayton cycle-based combined cycle for solar power tower plants. *Energy Convers Manag.* 2016;128:227–37.
50. Atif M, Al-Sulaiman FA. Energy and exergy analyses of solar tower power plant driven supercritical carbon dioxide recompression cycles for six different locations. *Renew Sustain Energy Rev.* 2017;68:153–67.
51. Korakianitis T, Wilson DG, editors. Models for predicting the performance of Brayton-cycle engines. ASME 1992 International Gas Turbine and Aeroengine Congress and Exposition; 1992: American Society of Mechanical Engineers.
52. Bergman TL, Incropera FP, Lavine AS, DeWitt DP. Introduction to heat transfer. New York: Wiley; 2011.
53. Turchi CS, Ma Z, Neises TW, Wagner MJ. Thermodynamic study of advanced supercritical carbon dioxide power cycles for concentrating solar power systems. *J Sol Energy Eng.* 2013;135(4):041007.
54. Cheng W-L, Huang W-X, Nian Y-L. Global parameter optimization and criterion formula of supercritical carbon dioxide Brayton cycle with recompression. *Energy Convers Manag.* 2017;150:669–77.
55. Cengel YA, Boles MA. Thermodynamics: an engineering approach. Sea. 2002;1000:8862.
56. Zareh AD, Saray RK, Mirmasoumi S, Bahlouli K. Extensive thermodynamic and economic analysis of the cogeneration of heat and power system fueled by the blend of natural gas and biogas. *Energy Convers Manag.* 2018;164:329–43.

**Publisher's Note** Springer Nature remains neutral with regard to jurisdictional claims in published maps and institutional affiliations.